IV Journeys in Multiphase Flows (JEM2015)
March 23-27, 2015 - Campinas, Brazil

PaperID: JEM-2015-0002

EXPERIMENTAL ANALYSIS OF THE ONSET OF FLOW REVERSAL IN UPFLOW CONDENSATION IN VERTICAL AND INCLINED TUBES

Daniel Hense
Júlio C. A. Ferreira
Jader R. Barbosa Jr.
POLO - Research Laboratories for Emerging Technologies in Cooling and Thermophysics (POLO), Department of Mechanical Engineering, Federal University of Santa Catarina (UFSC), Florianópolis, SC 88040900. Brazil
jrb@polo.ufsc.br

Abstract. *This work deals with an experimental analysis of the onset of flow reversal in upflow condensation of refrigerants in an inclinable small-diameter (5-mm ID) tube. As part of the condensate begins to flow downwards as a falling film, solitary waves grow on the liquid substrate and are carried upwards by the vapor. As a result of the periodic changes in liquid velocity, the vapor-liquid interface becomes highly disturbed, giving rise to significant liquid breakup from the crests of the waves and vapor entrainment in the liquid film. Image processing techniques have been applied to high-speed video sequences in order to identify the onset of flow reversal and to quantify the frequency and velocities of two-phase flow structures, such as disturbance waves and Sekoguchi-type huge waves characteristic of the transition to churn flow. Adaptations of existing correlations for the critical vapor velocity associated with the point of flow reversal have been proposed.*

Keywords: *Flow reversal, upflow condensation, flow structures, flow patterns, R-134a*

1. Introduction

The use of oil-free compressors in refrigeration systems creates new options for how the system components can be positioned relative to each other in the refrigerator. Oil-free compressors no longer need to be at the lowest position in the cooling circuit because oil return to the sump is no longer a design constraint. Nevertheless, although there is more freedom to position the heat exchangers relative to the compressor, some system configurations are more desirable than others to avoid condensate flow reversal in the condensing line.

The point of flow reversal in upward two-phase flow is defined as the point at which the momentum flux of the vapor phase is no longer capable of lifting the entire liquid phase up the channel. As a result, part of the liquid starts to flow downward and liquid flow velocity oscillations are observed. In large-diameter tubes where droplet entrainment is significant, flow reversals initially take place in the liquid film (van't Westende *et al.*, 2007) and is characterized by regions of falling liquid film between large upward moving waves (Hewitt *et al.*, 1985). The point of flow reversal has been associated with the point of minimum pressure drop in upward gas-liquid flow, and has been used as a criterion to correlate the transition from annular flow to churn flow in terms of the superficial gas velocity (Wallis, 1969).

In gas-liquid flows, the term *flooding* is used to describe the transition from a falling film flow to a bidirectional (upward and downward) flow, following an increase in gas velocity. In reflux condensation, flooding is said to occur when the condensate flow moves from a gravity-controlled regime to a shear-controlled regime (Sacramento and Heggs, 2009). As the upward gas velocity is further increased, the downward liquid flow rate is reduced until the liquid is totally carried upward. This condition is also known as the zero penetration limit (Wallis and Makkenchery, 1974). Hysteresis effects associated with the onset of flooding for increasing and decreasing gas flow rates have been discussed by Govan *et al.* (1991) and Shoukri *et al.* (1994).

Numerous correlations have been proposed for the critical gas velocity associated with flooding in vertical and inclined pipes. The correlation due to Wallis (1969) is given by:

$$(J_G^*)^{1/2} + m_1 (J_L^*)^{1/2} = C_1 \tag{1}$$

where J_k^* is a densimetric Froude number of phase k defined as:

$$J_k^* = J_k \left[\frac{\rho_k}{(\rho_L - \rho_G)\, g\, D} \right]^{1/2} \tag{2}$$

and m_1 and C_1 are empirical constants that depend on the test section geometry and flow inlet conditions. Typical values of m_1 and C_1 range from 0.5 to 1.0 and 0.7 to 1.0 (Govan *et al.*, 1991; Shoukri *et al.*, 1994).

The Tien-Kutateladze correlation (Tien, 1977; Kutateladze, 1972) is based on the Kutateladze numbers for each phase in the following form:

$$(Ku_G)^{1/2} + m_2 (Ku_L)^{1/2} = C_2 \tag{3}$$

where Ku_k is defined in terms of the Laplace length scale as follows:

$$Ku_k = J_k \left[\frac{\rho_k^2}{(\rho_L - \rho_G)\, g\, \sigma} \right]^{1/4} \tag{4}$$

where $m_2 \approx 1$ and $C_2 \approx 1.7 - 2$ are empirical constants (Ghiaasiaan, 2008).

Equations 1 and 3 can be used to predict the total carry-up (zero penetration) limit by setting the superficial liquid velocity terms to zero. The expression resulting from the Wallis correlation, $J_G^* = C_1^2$, suggests that the critical superficial gas velocity at the point of flow reversal is proportional to the square root of the tube diameter. The Tien-Kutateladze correlation, on the other hand, suggests that the critical gas velocity is independent of the tube diameter. The data of Pushkina and Sorokin (1969) for the zero penetration limit were correlated with $Ku_G \approx 3.2$. The classical Turner *et al.* (1969) correlation for the onset of liquid loading in gas wells suggests a critical Ku_G of approximately 3.67.

The apparent contradiction between the Wallis and Tien-Kutateladze correlations as regards the dependence of the critical superficial gas velocity on the tube diameter has been settled by Richter (1981), who found that the critical gas velocity was independent of the tube diameter only for large values of D (larger than 0.1 m). According to Hewitt (2010), for small-diameter tubes (less than 0.05 m in diameter) with smooth liquid inlets and outlets (e.g., a porous wall segment), flooding is initiated by a large coherent wave formed at the liquid outlet. For larger tubes, the waves formed are not coherent and the earliest mechanism of liquid transport is droplet entrainment from the tips of the waves. A number of empirical and semi-empirical flooding correlations have been presented for isothermal flows, which take into account the effects of channel geometry, inclination and physical properties (McQuillan and Whalley, 1985; Zapke and Kroeger, 1996, 2000b,a; Mouza *et al.*, 2005; Pantzali *et al.*, 2008). Comprehensive reviews have been presented by Bankoff and Lee (1986), Levy (1999) and Ghiaasiaan (2008).

Few authors investigated flooding and flow reversal phenomena in condensing refrigerants. Some fundamental differences can be identified when comparing these studies and those involving adiabatic flows of non-condensing substances: (i) the ratio of the liquid and vapor densities in condensing refrigerants is generally between 30 and 40, while the density ratio in water-air systems is of the order of 1000; (ii) in experiments without phase change, the liquid phase is injected and/or removed at specific points along the tube via small orifices or sintered segments of the tube. During condensation, the liquid phase is formed continuously along the tube. If the tube is inclined, then the condensation rate is not circumpherentially uniform; (iii) in order to identify the points of flooding and flow reversal in experiments without condensation, the phase flow rates are independently controlled. Usually, the liquid flow rate is kept fixed, while the gas flow rate is slowly increased or decreased. In upflow condensation experiments, the total mass flow rate is constant and vapor mass quality decreases along the test section. As a result, different flow regimes may exist simultaneously in the tube.

Fiedler and co-workers (Fiedler *et al.*, 2002, 2003; Fiedler and Auracher, 2004a,b) investigated flooding phenomena during reflux condensation of R-134a in vertical and inclined tubes (7-mm ID, 500-mm long). The flooding point was identified through a combination of an ultrasound measurements and flow visualization at the outlet of the test section. A specially-designed test section enabled measurements of the flow rate of condensate collected at the bottom. The optimum inclination angle corresponding to the maximum flooding velocity was between 45 and 60 from the horizontal. A mathematical model was proposed to determine the flooding velocity. Park and Mudawar (2013) studied upflow condensation of FC-72 in a 1.22-m long 10.16-mm ID vertical tube. High-speed video sequences were acquired to investigate the condensation flow regimes and local heat transfer coefficients were determined for the various flow regimes. The onset of film flow reversal was correlated using the Wallis (1969) flooding relationship.

The objective of the present paper is to investigate the onset of flow reversal and the characteristics of flow structures (interfacial waves) in upflow condensation of R-134a in a 5-mm ID, 950-mm long inclinable tube. The experimental facility is a R-134a vapor compression refrigeration cycle equipped with an oil-free compressor. Flow visualization is performed using high-speed video sequences acquired at a distance of 855 mm from the refrigerant inlet. Algorithms have been developed to determine the frequencies and velocities of the interfacial waves based on the digital images. The onset of flow reversal is correlated using the Wallis approach and compared with data from the literature.

2. Experimental Work

2.1 Experimental Setup

The experimental apparatus is represented schematically in Fig. 1. It consists of a R-134a vapor compression refrigeration cycle equipped with an oil-free compressor. The test section (1) is a transparent counterflow tubular heat exchanger, which will be described in detail in Section 2.2 The refrigerant enters the test section with a specified superhating degree and is partially condensed, leaving it as a two-phase mixture. Temperature measurements in the flow loop are carried out using Pt-100 RTDs (2), with expanded uncertainties ranging from 0.12 °C to 0.14 °C. The refrigerant pressure drop between the inlet and outlet of the test section is measured with a Rosemount 6051S differential pressure transducer (3), with an uncertainty of 4.0 Pa.

The two-phase mixture leaving the test section is condensed in a brazed plate heat exchanger (Alfa Laval CBH16-9H) (4) and exits the condenser with a subcooling degree of $4\,^{\circ}$C. The refrigerant flow rate is measured with a Coriolis effect mass flow meter (Micromotion CFMS010) (5) with an uncertainty of 9.0×10^{-6} kg/s. The expansion device consists of a Swagelok SS-31RS4 metering valve mounted in series with and a 0.3-m long, 1.08-mm ID capillary tube. The evaporating section consists of a 450-W resistance heater wrapped around a 9.52-mm (3/8") copper tube. The refrigerant in superheated to $10\,^{\circ}$C above the evaporating temperature as it exits the evaporator.

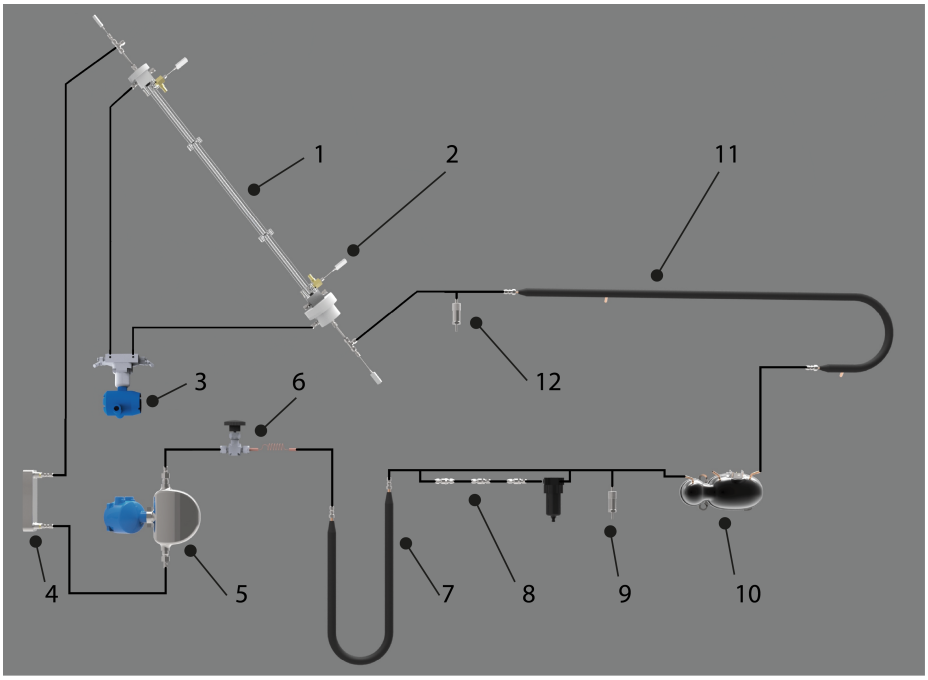

Figure 1: Schematic diagram of the experimental apparatus: flow loop and main equipment.

A set of coalescent and particulate filters (8) was installed in a bypass to keep the refrigerant free from moisture and impurities. These are used periodically, especially when refrigerant mass is added to the system. The evaporating pressure is measured with an absolute pressure transducer (9) (Wika P-30-6) mounted upstream of the oil-free compressor (10). The combined uncertainty of the evaporating pressure measurement is 0.254 kPa. The high-pressure refrigerant is discharged into a double pipe heat exchanger (11), which is responsible for guaranteeing a fixed superheating degree of $2\,^{\circ}$C at the inlet of the test section. The condensing pressure is measured with a Wika P-30-16 absolute pressure transducer (12) with a combined uncertainty of 0.446 kPa. A glycol solution was used as a coolant in the test section and high-pressure heat exchangers. Three independent thermal baths (one for each heat exchanger) were used.

2.2 Test Section

The test section, presented in detail in Fig. 2, is divided in three sections: (i) inlet header, (ii) heat exchanger and (iii) outlet header. Figure 3 shows a cutaway view of the inlet header. To reduce the experimental errors to a minimum, the differential pressure taps in the inlet and outlet headers were machined following the recommendations of (Benedict, 1984). The inlet and outlet temperatures of the glycol solution (secondary fluid) were measured in a 90° bend to take advantage of fluid mixing. The mass flow rate of the secondary fluid in the test section was measured with a Contech FM-8-7 turbine flow meter, with a combined uncertainty of 1.6×10^{-4} kg/s.

The length of the heat exchanger section is 950 mm. The inner tube is made from borosilicate glass with an internal diameter, D of 5 mm and wall thickness of 1 mm. The glycol solution flows through the annular gap between the outer wall of the inner tube and the inner wall of a transparent acrylic resin (outer) duct. The internal diameter of the outer duct is 11 mm, resulting in a hydraulic diameter of 4 mm for the annular gap. The outer surfaces of the outer duct are flat (square cross section) to improve visualization of the two-phase condensing flow inside the inner duct. The outer duct was divided into three parts connected by flat-face bolted flanges to facilitate assembling of the test section. The test section is mounted on a rigid frame, which can be inclined at specified angles from the horizontal.

2.3 Experimental procedure

Experimental tests were carried out varying the condensing pressure of R-134a (830 and 1040 kPa), test section inclination from horizontal (30, 60 and 90°), inlet superheating degree (2, 10 and 20 °C) and condensation (heat transfer) rate

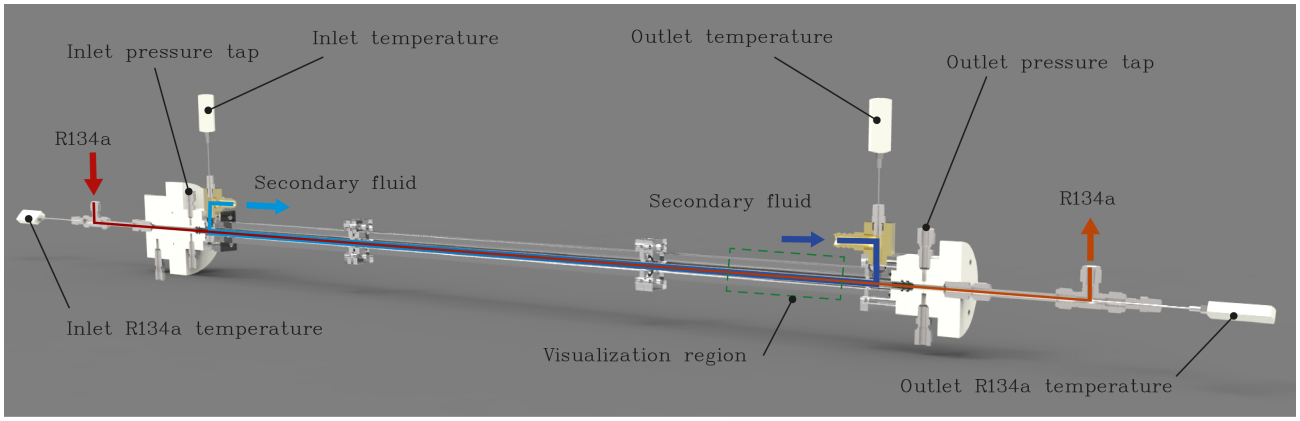

Figure 2: Test section.

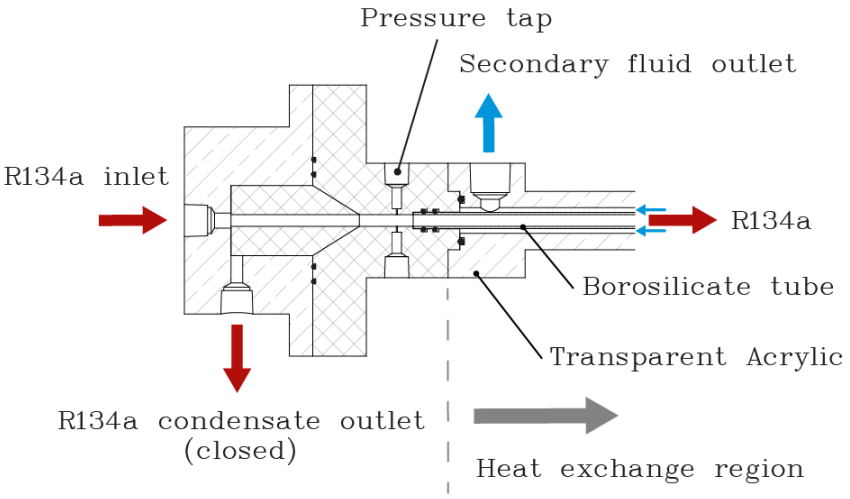

Figure 3: Inlet header.

in the test section (30 to 190 W). The condensation rate is controlled by the secondary fluid flow rate or inlet temperature. The refrigerant flow rate is, therefore, a dependent variable in the experiments. In total, 264 experimental points were generated.

An experimental condition is defined by a given condensing pressure, inclination and inlet superheating degree. Several tests were conducted for different conditions by changing the condensation rate. The tests were carried out increasing the condensation rate, and the first test for a given experimental condition always guaranteed a unidirectional, climbing film flow near the outlet of the test section where the flow visualization region was located (see Fig. 2), i.e., $J^*_{G,o} \approx 1.4$. For each subsequent test, the condensation rate was increased so as to reduce $J^*_{G,o}$ in steps of 0.1 until the maximum condensation rate is reached.

The experiments were divided into two groups. In the first group, the mass of refrigerant in the system (i.e., the refrigerant charge) was kept fixed. Increasing the test section condensation rate at a fixed refrigerant charge reduced both the condensing pressure and the refrigerant mass flow rate as a result of the progressive accumulation of refrigerant (in the form of liquid condensate) in the test section. In the second group, the refrigerant charge was adjusted for each test (with the help of a refrigerant charging cylinder connected to the experimental apparatus) so as to maintain the same refrigerant mass flow rate irrespective of the condensation heat transfer rate. While the first group represents the behavior of actual vapor compression refrigeration systems in which the oil-free compressor is used, the second group is more appropriate for evaluating the effect of changing the flow conditions on two-phase flow parameters, such as the pressure drop and wave velocities. In the present paper, data from the first group were used only for qualitative purposes (e.g., illustration of the phase distribution in the channel). Quantitative analyses were carried out using data from the second group only.

Data logging was performed using National Instruments hardware and the Labview software. The sampling frequency of the pressure and mass flow rate data was 2 kHz, which is significantly higher than the frequencies of the two-phase flow structures (disturbance waves, liquid slugs). After the desired operating conditions are set, approximately 90 minutes are required to achieve stable operation of the experimental apparatus for a given test. The steady state criterion was defined based on the existence of a 10-min period of continuous operation with the fluctuations of all experimental parameters

being smaller than their respective combined experimental uncertainties.

The high-speed video sequences of the two-phase flow were acquired at 3 kHz using a Phantom V12 high-speed camera equipped with a Zeiss Makro Planar T* 2/100 lens. The flow visualization region of the test section was positioned at 855 mm from the inlet of the test section, as seen in Fig. 2. The flow was illuminated by three 130-W (60 kLux) 19-LED systems manufactured by IDT Inc.

For a given test, the frequency of the flow structures was determined by counting the number of frames, n, between consecutive structures observed at a specified position along the test section. The frequency is calculated as the average of N intervals between structures as follows:

$$f = \frac{f_{aq}}{N} \sum_{i=1} N n_i \tag{5}$$

where the minimum value of N was equal to 6 to preserve the statistical significance of the results.

The structure velocity was calculated using a similar algorithm, taking the external diameter of the internal tube as a reference length scale. The structure velocity is proportional to the number of pixels associated with its displacement over a given number of consecutive time frames, n. Again, the data were averaged for at least 6 structures.

2.4 Data regression

The inlet velocity of the superheated vapor in the test section is calculated from the experimental mass flow rate as follows:

$$J_{G,i} = \frac{4\,\dot{m}_r}{\pi\,D^2\,\rho_{G,i}} \tag{6}$$

where $\rho_{G,i}$ is the vapor density at the inlet calculated from the test section inlet pressure, P_i, and temperature, T_i, using Refprop 8.0 (Lemmon *et al.*, 2007).

The superficial velocities of the liquid and vapor phases at the outlet of the test section, $J_{L,o}$ and $J_{G,o}$, were determined based on the local vapor quality calculated from an energy balance in the test section. Neglecting the small heat losses to the ambient, the vapor quality at the outlet of the test section, x_o, is given by:

$$x_o = \frac{\dot{m}_r - \left(\dot{Q}_{cond}/h_{LG}\right)}{\dot{m}_r} \tag{7}$$

where h_{LG} is the enthalpy of vaporization of R-134a and $\dot{Q}_{cond}$ is the condensation heat transfer rate given by:

$$\dot{Q}_{cond} = \dot{m}_{fs}\,cp_{fs}\,(T_{s,fs} - T_{e,fs}) - \dot{m}_r\,cp_{r,G,e}\,(T_1 - T_{sat}) \tag{8}$$

where the first term on the left is the total heat transfer rate in the test section measured in the secondary fluid and the second term is the heat transfer rate required to desuperheat the refrigerant as it enters the test section. The specific heat capacity of the glycol solution (secondary fluid) was obtained from tabulated data.

The vapor and liquid superficial velocities at the outlet of the test section are calculated from:

$$J_{G,o} = \frac{4\,x_o\,\dot{m}_r}{\pi\,D^2\,\rho_{G,o}} \tag{9}$$

$$J_{L,o} = \frac{4\,(1-x_o)\,\dot{m}_r}{\pi\,D^2\,\rho_{L,o}} \tag{10}$$

The local dimensionless superficial velocities, J_G^* and J_L^*, were calculated from Eq. 2.

3. Results

3.1 Flow pattern visualization

Figures 4 and 5 show sequences of images acquired at a nominal total mass flux (mass flow rate per unit area) of 77 kg/m^{2}s for a condensing pressure of 1040 kPa and inclinations of 90 and 60°, respectively. The time interval between consecutive frames is 3.33 ms. The sequences of images are organized in order of increasing liquid content, or decreasing vapor quality. Five distinct regions have been identified, namely, (i) climbing film flow, (ii) stationary film flow, (iii) flow reversal, (iv) churn flow and (v) slug flow. In each sequence, lines are used to identify the displacement of a given flow structure as a function of time. Orange (solid) lines represent upward flowing structures, green (dashed) lines are used

to identify structures that remain approximately stationary and blue (dotted) lines indicate downward-flowing liquid film structures. Particular features of each region will be described next.

At the highest local vapor qualities of Figs. 4(a) and 5(a), there is unidirectional flow in both phases, and disturbance waves on the liquid film are observed to travel at an approximately constant velocity. In Fig. 5(a), the disturbance waves are already clearly thicker at the bottom of the tube (right-hand side of each image) due to the gravity component in the radial direction. As will be seen in the figures, radial asymmetry tends to increase with the decrease in vapor quality and reduction of the inertia of the vapor phase.

As the condensation rate is increased, film gravity is cancelled out by the interfacial drag in some parts of the liquid film. As a result, the film is partly stationary while other parts (disturbance waves) are clearly moving upward, as shown in Fig. 4(b). Similar behavior can be identified in Fig. 5(b) for an inclination of 60°, where the lack of radial symmetry in the liquid is evident. In both cases, the orange lines are no longer parallel, meaning that different parts of the film flow with different velocities.

The onset of film flow reversal depicted in Figs. 4(c) and 5(c) is characterized by the existence of downward flow in certain portions of the liquid film. In this case, the amount of condensate is already large enough so that the gravity force locally exceeds the interfacial drag. As clearly observed in Figs. 4(c) and 5(c), the downward flow persists until a larger upward-moving wave (with more momentum) engulfs the first wave, as illustrated by the crossing of the blue (dotted) and orange (solid) lines. Continuous observation of the flow indicated that smaller waves tend to stop and flow downward (counter-current) more easily than larger waves. Despite of larger gravity force, two factors favor large waves to flow co-currently. Firstly, larger waves create narrower cross sections for the vapor flow, leading to higher local vapor velocities at the crest of the wave (Bernoulli effect), which increases the frictional drag. Secondly, the pressure difference between the windward and leeward sides of the wave helps to propel the wave upwards due to the increase in form drag.

At higher condensation rates, the occurrence of flow reversals is more pronounced and the so-called huge waves (Sekoguchi and Takeishi, 1989) are formed. These are typical of the transition from unidirectional to bidirectional flow in the liquid film that characterizes the transition to churn flow. The chaotic behavior of this flow regime is illustrated by the multitude of lines in Figs. 4(d) and 5(d). Even for the short duration of each sequence (0.0533 s), an intermittent behavior can be clearly observed, which consists of the following sequence of (i) downward wavy flow, (ii) condensate accumulation and (iii) climbing solitary wave (Hewitt *et al.*, 1985). The slug flow regime is illustrated in Figs. 4(e) and 5(e) for tube inclinations of 90° and 60°, respectively. This regime is characterized by the disappearance of the continuous vapor core and the formation of elongated vapor bubbles (Taylor bubbles), which are surrounder by regions of falling film.

3.2 Flow pattern map

Each sequence of high-speed images was carefully analyzed to determine the corresponding two-phase flow pattern. The results were plotted as flow pattern maps to better identify the transitions between the flow regimes. In order to be minimally consistent with previous works (Park and Mudawar, 2013), four regimes have been used to classify the experimental data, namely, (i) climbing film, (ii) flow reversal, (iii) churn flow and (iv) slug flow. It should be noted that the flow reversal regime encompasses both the stationary film and flow reversal regions identified in Figs. 4 and 5, as sometimes the transition between them can be quite subtle and prone to some degree of subjectivity. For this reason, the passage from climbing film flow to flow reversal usually spanned between 2 and 4 tests for each experimental condition.

The criterion for churn flow was the occurrence of significant counter-current flow, leading to the formation of a solitary (huge) wave. A huge wave is considered to be formed when its crest touches the opposite wall of the tube or the crest of another wave. Slug flow was formed when a Taylor bubble was clearly identified, resulting in blockage of the test section by a liquid slug.

Figure 6 compares the present experimental observations for the transitions between flow regimes in a vertical tube with the predictions of Park and Mudawar (2013) of the flow regimes they identified as climbing film, flooding, oscillating film and falling film. There is good agreement between the two data sets at the transition from the climbing to the flow reversal (stationary film) and flooding regimes (Park and Mudawar, 2013). The transition to the oscillating film regime of Park and Mudawar (2013) also agrees well with the transition to what has been identified in this study as churn flow. Indeed, the sequential images of the falling film regime of Park and Mudawar (2013) are very similar to those associated with churn flow in Figs. 4 and 5. The small but noticeable influence of the liquid flow rate on the transition between the flow regimes was also similar for the two data sets, with the critical dimensionless vapor velocity decreasing with the liquid flow rate. The data of Fiedler *et al.* (2002) for the flooding limit in reflux condensation of R-134a in a 7-mm ID, 50-mm long tube is also shown for comparison purposes. As expected, these lie below the flow reversal transition due to the higher momentum of the vapor flow required to reach the zero penetration limit (Wallis and Makkenchery, 1974).

Predictions of flow regime transitions by Wallis-type correlations are presented in Fig. 7 for tube inclinations of 90, 60 and 30° with the horizontal. In each figure, data for condensing pressures of 830 and 1040 kPa are shown. Three different sets of constants are exhibited in an attempt to correlate the different transitions. The curves drawn with $C = 1.72$ and $m = 1.0$ predict well the transition from the climbing film to the flow reversal (stationary film) regions for all inclinations. The constants suggested by Park and Mudawar (2013) for their flooding-oscillating film transition, namely $C = 1.21$ and

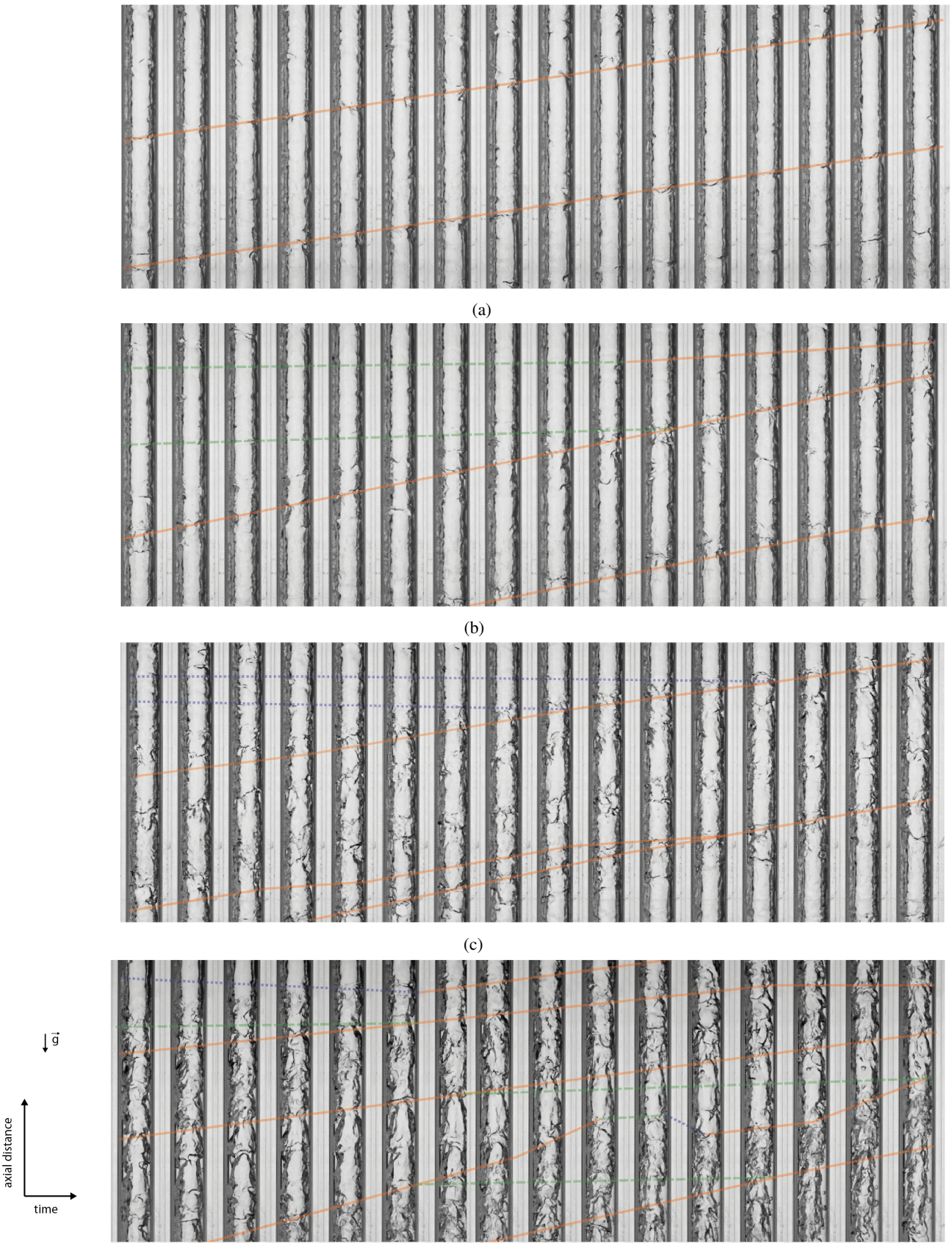

Figure 4: Continued.

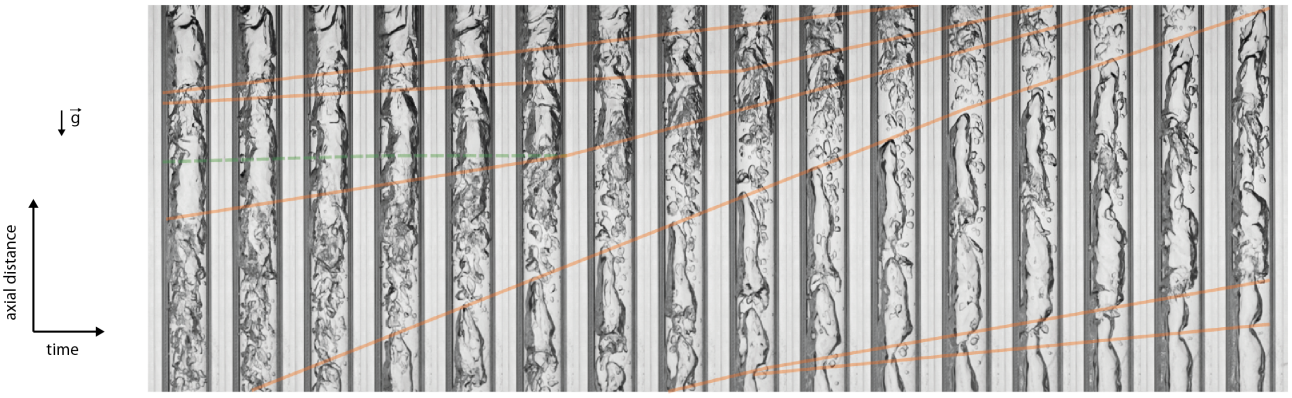

(e)

Figure 4: High-speed video sequences for a condensing pressure of 1040 kPa, nominal total mass flux of 77 kg/m^2.s and 90° from the horizontal. The images were obtained at a distance of 855 mm from test section inlet. (a) Climbing film flow, $x_o = 0.86$, $J^*_{G,o}$ =1.28 and $J^*_{L,o}$ =0.05. (b) Stationary film flow, $x_o = 0.81$, $J^*_{G,o}$ =1.14 and $J^*_{L,o}$ =0.08, (c) Flow reversal, $x_o = 0.61$, $J^*_{G,o}$ =0.88 and $J^*_{L,o}$ =0.13, (d) Churn flow, $x_o = 0.41$, $J^*_{G,o}$ =0.54 and $J^*_{L,o}$ =0.20, (d) Slug flow, $x_o = 0.28$, $J^*_{G,o}$ =0.32 and $J^*_{L,o}$ =0.24.

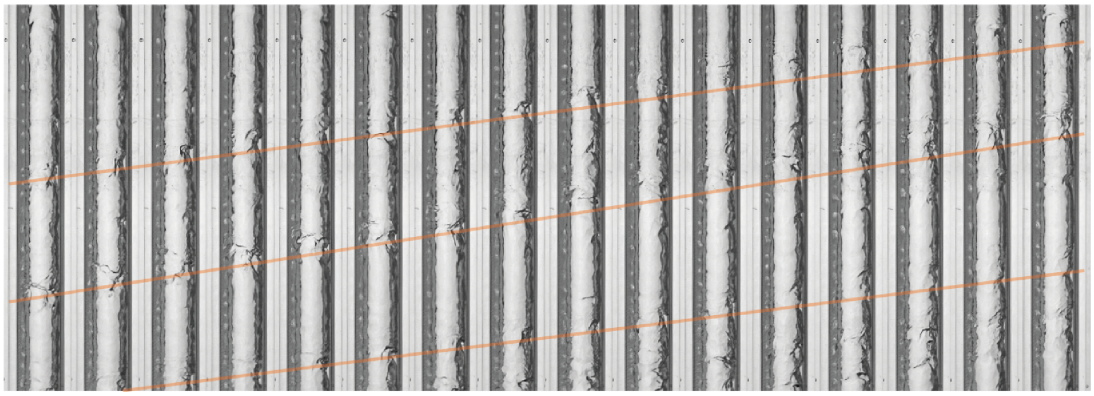

(a)

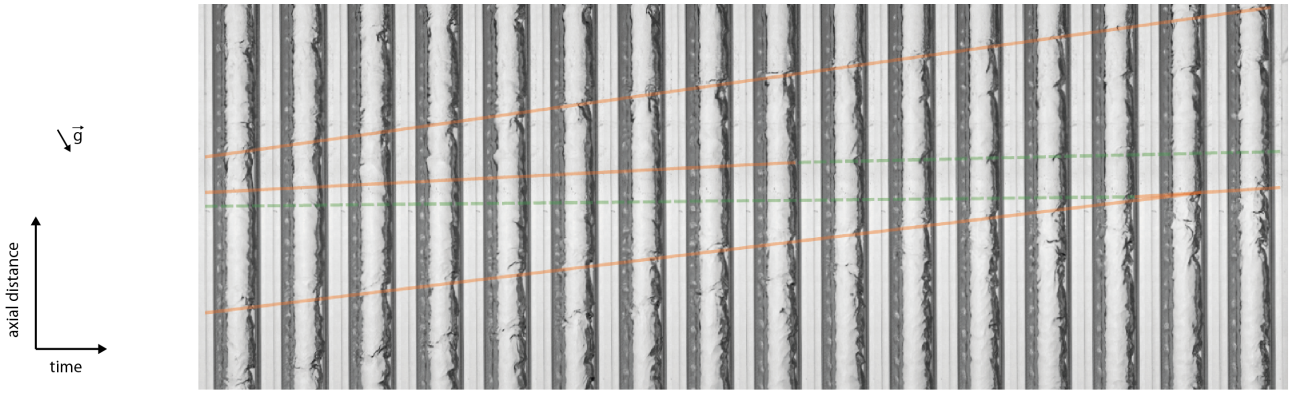

(b)

Figure 5: Continued.

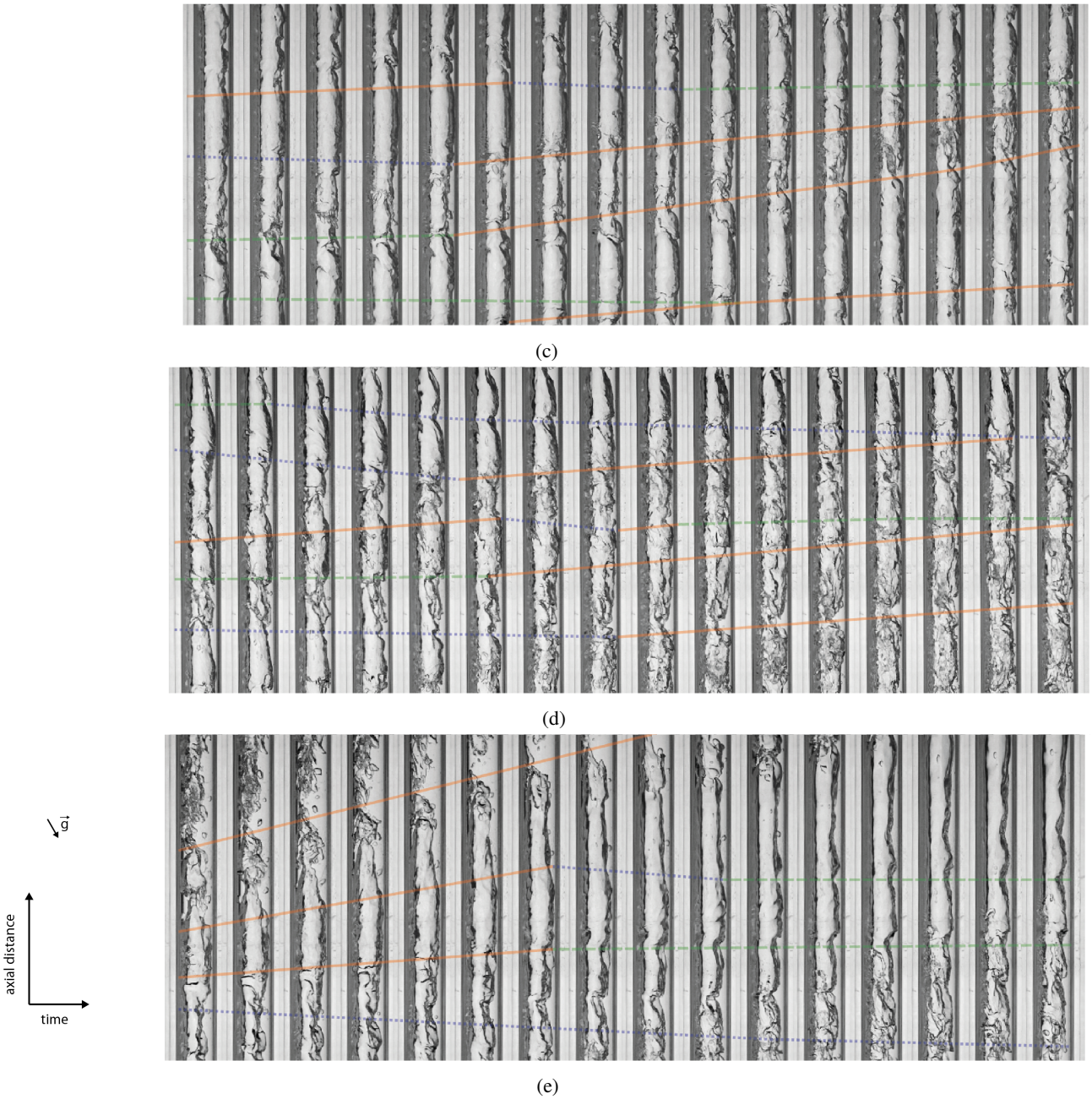

Figure 5: High-speed video sequences for a condensing pressure of 1040 kPa, nominal total mass flux of 78 kg/m^2.s and 60° from the horizontal. The images were obtained at a distance of 855 mm from test section inlet. (a) Climbing film flow, $x_o = 0.86$, $J^*_{G,o}$ =1.27 and $J^*_{L,o}$ =0.05, (b) Stationary film flow, $x_o = 0.75$, $J^*_{G,o}$ =1.10 and $J^*_{L,o}$ =0.09, (c) Flow reversal, $x_o = 0.61$, $J^*_{G,o}$ =0.83 and $J^*_{L,o}$ =0.13, (d) Churn flow, $x_o = 0.41$, $J^*_{G,o}$ =0.54 and $J^*_{L,o}$ =0.20, (d) Slug flow, $x_o = 0.26$, $J^*_{G,o}$ =0.30 and $J^*_{L,o}$ =0.25.

$m = 1.0$, slightly over predict the transition to churn flow in vertical flow. In this situation, better agreement was achieved with $C = 1.0$ and $m = 1.0$ (Wallis, 1969), which were used by Park and Mudawar (2013) to correlate the transition to their falling film regime. However, for 60 and 30° with the horizontal, $C = 1.21$ and $m = 1.0$ do a resonably good job at predicting the transition to churn flow. It should be mentioned that the acceleration of gravity, g, has been replaced $g \sin\theta$ in the calculation of the superficial phase velocities J^*_G and J^*_L for the 60 and 30° inclinations.

3.3 Characterization of flow structures

Figure 8(a) presents results of frequencies of flow structures as a function of the outlet vapor mass flux G_G. There is no clear effect of pressure or tube inclination. As observed by Han *et al.* (2006), the structure frequency tends to increase with vapor superficial velocity. This trend is also observed when f is plotted against the Weber number We, as presented

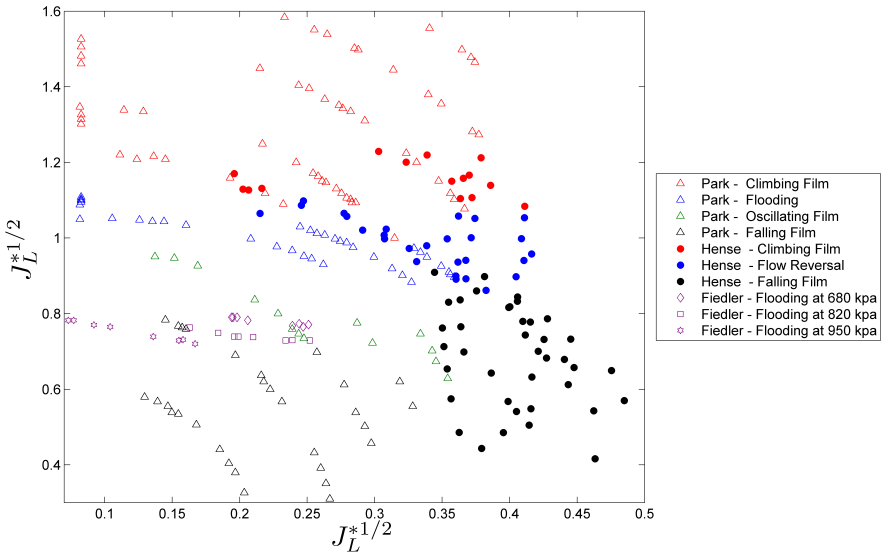

Figure 6: Comparison between current experimental points for vertical tube with Park and Mudawar (2013) and Fiedler *et al.* (2002) data.

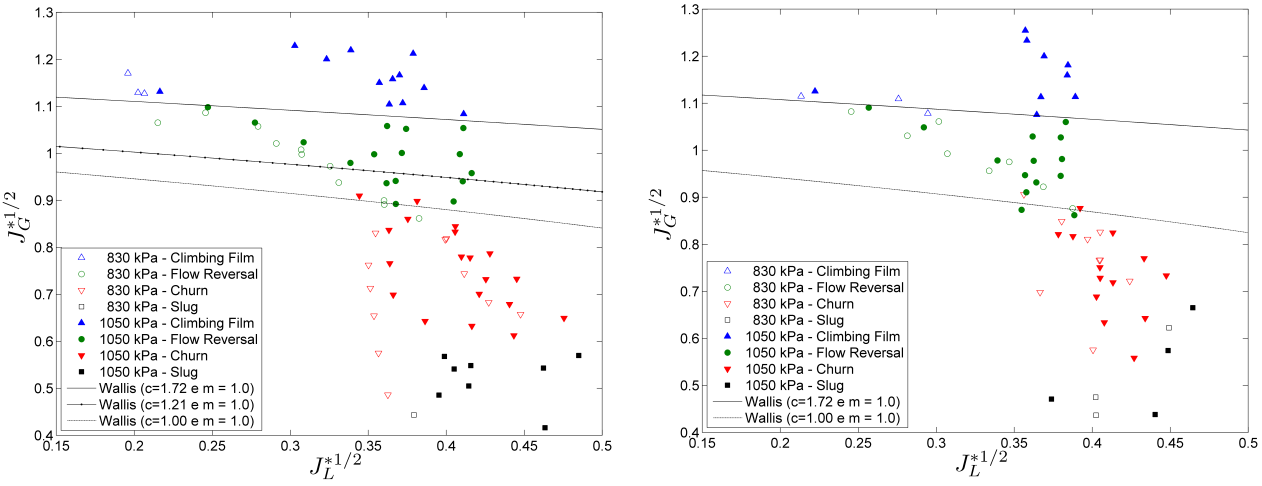

(a) Vertical tube

(b) 60° inclined tube

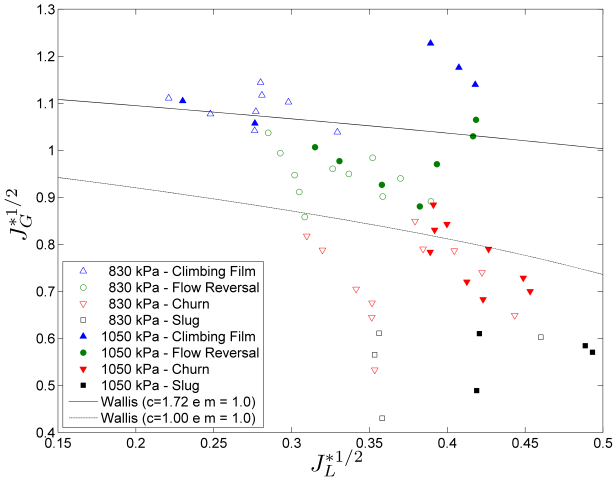

(c) 30° inclined tube

Figure 7: Flow pattern map for internal diameter 5 mm and Wallis correlation with different constants.

in Fig. 8(b). This figure shows a stronger increase of f with We for churn and slug flow patterns, but less so for annular flow f. The different trends for intermittent (churn and slug) and annular patterns were also identified by Sawant *et al.* (2008). The Weber number is defined as,

$$We = \frac{\rho_G \, J_G^2 \, D}{\sigma} \left(\frac{\rho_L - \rho_G}{\rho_G} \right)^{1/3} \tag{11}$$

and denotes the relative importance of inertial and surface tension forces.

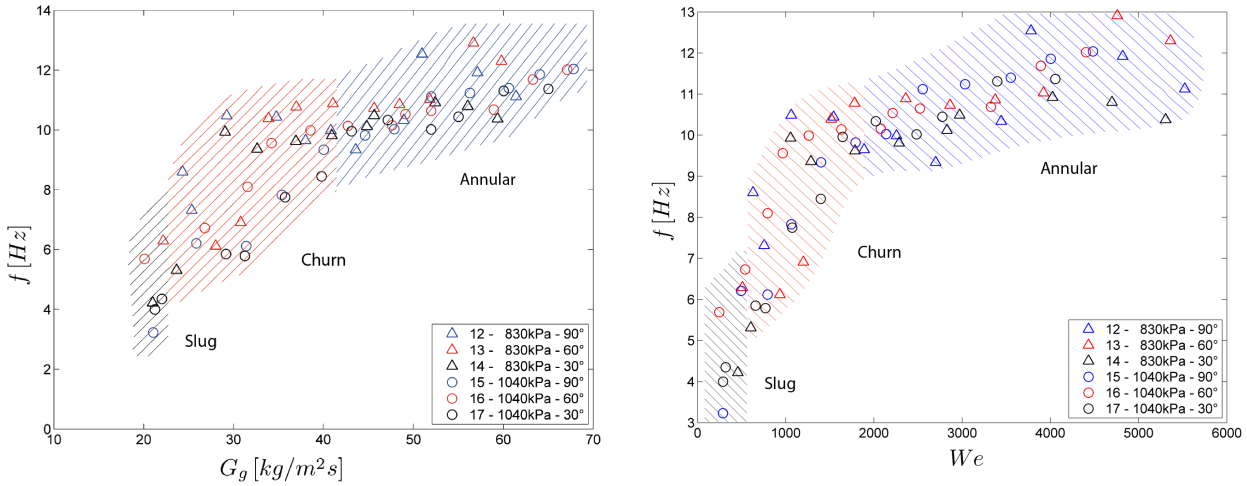

(a) Frequency f as function of outlet vapor mass flux G_G. (b) Frequency f as function of Weber number We.

Figure 8: Experimental results for flow structure frequency

The flow structure velocity data are presented in Fig. 9 as V_{struc}/J_G per J_L. For annular pattern V_{struc}/J_G increases linearly with J_L, as observed by Schubring and Hurlburt (2010). For churn and slug flow larger dispersion is observed, possibly due intermittent behavior, and much larger V_{struc}/J_G values are observed.

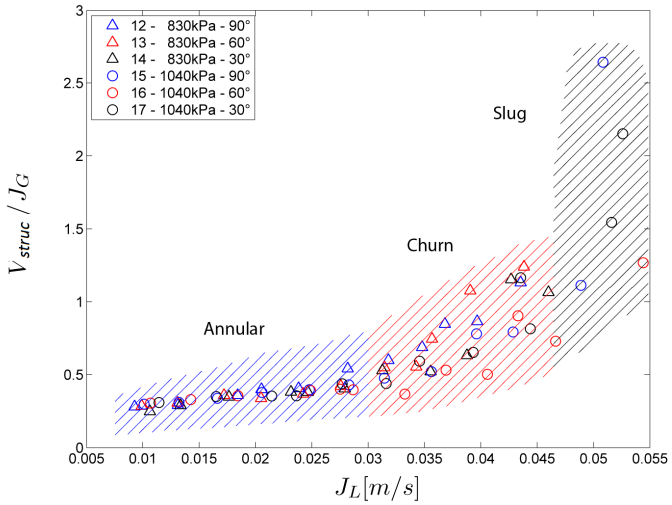

Figure 9: Experimental data for structure velocity per gas superficial velocity as function of liquid superficial velocity.

4. Conclusion

This study explored the flow regimes involved in the counter-current flow limitation transitions (flooding and flow reversal) and flow structure characterization encountered in upward flow with condensation of R-134a in an inclinable small diameter tube. Two condensing pressures and three inclinations were investigated, totalling 264 experimental points. High frequency image acquisition was used to examine flow transitions and flow structures. Flow and temperature measurements were used to estimate gas and liquid dimensionless superficial velocity at test section outlet, in order to construct flow regime maps. Flow regime maps based on the Wallis dimensionless superficial velocities showed good

agreement with flow regime transitions. Coefficients $C = 1.72$ and $m = 1.0$ yielded good agreement with the transition between the climbing film regime and flow reversal. Additionally, different trends for flow structure frequency and velocity were observed for annular and intermittent (churn and slug) flow regimes.

5. Acknowledgements

Financial support from Embraco and CNPq (National Institute of Science and Technology in Cooling and Thermophysics) is duly acknowledged.

6. References

Bankoff, S.G. and Lee, S.C., 1986. "A critical review of the flooding literature". *Multiphase Science and Technology*, Vol. 2, pp. 95–180.

Benedict, R.P., 1984. *Fundamentals of temperature, pressure and air flow measurement*. John Wiley & Sons.

Fiedler, S. and Auracher, H., 2004a. "Experimental and theoretical investigation of reflux condensation in an inclined small diameter tube". *International Journal of Heat and mass Transfer*, Vol. 47, pp. 4031–4043.

Fiedler, S. and Auracher, H., 2004b. "Pressure drop during reflux condensation of r134a in a small diameter tube". *Experimental Thermal and Fluid Science*, Vol. 28, pp. 139–144.

Fiedler, S., Auracher, H. and Winkelmann, D., 2002. "Effect of inclination on flooding and heat transfer during reflux condensation in small diameter tube". *International Communications of Heat and Mass Transfer*, Vol. 29, pp. 289–302.

Fiedler, S., Yildiz, S. and Auracher, H., 2003. "Determination of film thickness and flooding during reflux condensation in a small, inclined tube with an ultrasonic transducer". *International Journal of Energy Research*, Vol. 27, pp. 315–325.

Ghiaasiaan, S.M., 2008. *Two-Phase Flow, Boiling and Condensation*. Cambridge.

Govan, A.H., Hewitt, G.F., Richter, H.J. and Scott, A., 1991. "Flooding and churn flow in vertical pipes". *International Journal of Multiphase Flow*, Vol. 17, No. I, pp. 27–44.

Han, H., Zhu, Z. and Gabriel, K., 2006. "A strudy on the effect of gas flow rate on the wave characteristics in two-phase gas-liquid annular flow". *Nuclear Engineering and Design*, Vol. 236, pp. 2580–2588.

Hewitt, G.F., Martin, C.J. and Wilkes, N.S., 1985. "Experimental and modelling studies of annular flow in the region between flow reversal and the pressure drop minimum". *Physico-Chemical Hydrodynamics*, Vol. 6, pp. 43–50.

Hewitt, G., 2010. "Flooding and flow reversal". In G.F. Hewitt and J.R. Barbosa Jr., eds., *Thermopedia*, Begell House, Inc. 10th edition.

Kutateladze, S.S., 1972. "Elements of hydrodynamics of gas-liquid systems". *Fluid Mechanics Soviet Research*, Vol. 1, pp. 29–50.

Lemmon, E.W., McLinden, M.O. and Huber, M.L., 2007. "REFPROP: Reference fluid thermodynamic and transport properties". *NIST standard reference database*, Vol. 23, No. 8.0.

Levy, S., 1999. *Two-phase flow in complex systems*. John Wiley & Sons.

McQuillan, K.W. and Whalley, P.B., 1985. "A comparison between flooding correlations and experimental flooding data for gas-liquid flow in vertical circular tubes". *Chemical Engineering Science*, Vol. 40, pp. 1425–1440.

Mouza, A.A., Pantzali, M.N. and Paras, S.V., 2005. "Falling film and flooding phenomena in small diameter vertical tubes: The influence of liquid properties". *Chemical Engineering Science*, Vol. 60, pp. 4987–4991.

Pantzali, M.N., Mouza, A.A. and Paras, S.V., 2008. "Counter-current gas-liquid flow and incipient flooding in inclined small diameter tubes". *Chemical Engineering Science*, Vol. 63, pp. 3966–3978.

Park, I. and Mudawar, I., 2013. "Climbing film, flooding and falling film bahavior in upward condensation". *International Journal of Heat and Mass Transfer*, Vol. 65, pp. 44–61.

Pushkina, O.L. and Sorokin, Y.L., 1969. "Breakdown of liquid film motion in vertical tubes". *Heat Transfer Soviet Research*, Vol. 1, pp. 56–64.

Richter, H.J., 1981. "Flooding in tubes and annuli". *International Journal of Multiphase Flow*, Vol. 7, No. 6, pp. 647–658.

Sacramento, J.C. and Heggs, P.J., 2009. "The role of flooding in the design of vent and reflux condensers". *Applied Thermal Engineering*, Vol. 29, pp. 1338–1345.

Sawant, P., Ishii, M., Hazuki, T., Takamasa, T. and Mori, M., 2008. "Properties of disturbance waves in vertical annular two-phase flow". *Nuclear Engineering and Design*, Vol. 238, pp. 3528–3541.

Schubring, D. and Hurlburt, T.A., 2010. "Studying disturbance waves in vertical annular flow with high-speed video". *International Journal of Multiphase Flow*, Vol. 36, pp. 385–396.

Sekoguchi, K. and Takeishi, M., 1989. "Interfacial structures in upward huge wave flow and annular flow regimes". *International Journal of Multiphase Flow*, Vol. 15, pp. 195–305.

Shoukri, M., Abdul-Razzak, A. and Yan, C., 1994. "Hysteresis effects in countercurrent gas-liquid flow limitations in a vertical tube". *The Canadian Journal of Chemical Engineering*, Vol. 72, pp. 576–581.

Tien, C.L., 1977. "A simple analytical model for countercurrent flow limiting phenomena with vapor condensation".

Letters in Heat and Mass transfer, Vol. 4, pp. 231–238.

Turner, R.G., Hubbard, M.G. and Dukler, A.E., 1969. "Analysis and prediction of minimum flow rate for the continuous removal of liquids from gas wells". *Journal of Petroleum Technology*, Vol. November, pp. 1475–1482.

van't Westende, J., Kemp, H., Belt, R., Portela, L., Mudde, R. and Oliemans, R., 2007. "On the role of droplets in cocurrent annular and churn-annular pipe flow". *International Journal of Multiphase Flow*, Vol. 33, p. 595ÃŘ615.

Wallis, G.B., 1969. *One-Dimensional Two-Phase Flow*. McGraw-Hill.

Wallis, G.B. and Makkenchery, S., 1974. "The hanging film phenomenon in vertical annular two-phase flow". *Journal of Fluids Engineering*, Vol. 96, pp. 297–298.

Zapke, A. and Kroeger, D.G., 1996. "The influence of fluid properties and inlet geometry on flooding in vertical and inclined tubes". *International Journal of Multiphase Flow*, Vol. 3, pp. 461–472.

Zapke, A. and Kroeger, D.G., 2000a. "Countercurrent gas-liquid flow in inclined and vertical ducts - i: Flow patterns, pressure drop characteristics and flooding". *International Journal of Multiphase Flow*, Vol. 26, pp. 1439–1455.

Zapke, A. and Kroeger, D.G., 2000b. "Countercurrent gas-liquid flow in invlined and vertical ducts - ii the validity of the froude-ohnesorge number correlation for flooding". *International Journal of Multiphase Flow*, Vol. 26, pp. 1457–1468.